Effects of Internal and External Pressure on the [Fe(PM-PEA)2(NCS)2] Spin-Crossover Compound (with PM-PEA = N-(2'-pyridylmethylene)-4-(phenylethynyl)aniline)

Nicolas Paradis, Frédéric Le Gac, Philippe Guionneau, Alain Largeteau, Dmitry Yufit, Patrick Rosa, Jean-François Létard, Guillaume Chastanet

magnetochemistry

MDPI

Article

Effects of Internal and External Pressure on the $[Fe(PM\text{-}PEA)_2(NCS)_2]$ Spin-Crossover Compound (with PM-PEA = *N*-(2′-pyridylmethylene)-4-(phenylethynyl)aniline)

Nicolas Paradis [1], Frédéric Le Gac [1], Philippe Guionneau [1,*], Alain Largeteau [1], Dmitry S. Yufit [2], Patrick Rosa [1], Jean-François Létard [1] and Guillaume Chastanet [1,*]

[1] CNRS, Univ. Bordeaux, ICMCB, UPR9048, 87 Avenue du Dr. Schweitzer, F-33600 Pessac, France; nicolas.paradis33@gmail.com (N.P.); guio@icmcb-bordeaux.cnrs.fr (F.L.G.); alain.largeteau@icmcb.cnrs.fr (A.L.); patrick.rosa@icmcb.cnrs.fr (P.R.); letard@olikrom.com (J.-F.L.)

[2] Department of Chemistry, University Science Laboratories, South Road, Durham—DH1 3LE, UK; d.s.yufit@durham.ac.uk

* Correspondence: philippe.guionneau@icmcb.cnrs.fr (P.G.); guillaume.chastanet@icmcb.cnrs.fr (G.C.); Tel.: +33-540002579 (P.G.); +33-540008323 (G.C.)

Academic Editors: Guillem Aromí and José Antonio Real
Received: 15 January 2016; Accepted: 29 February 2016; Published: 4 March 2016

Abstract: The spin-crossover properties of the strongly cooperative compound $[Fe(PM\text{-}PEA)_2(NCS)_2]$ (with PM-PEA = *N*-(2′-pyridylmethylene)-4-(phenylethynyl)aniline) have been investigated under external *in situ* pressure, external *ex situ* pressure and internal pressure. *In situ* single-crystal X-ray diffraction investigations under pressure indicate a Spin-Crossover (SCO) at about 400 MPa and room temperature. Interestingly, application of *ex situ* pressure induces the irreversible enlargement of the hysteresis width, almost independently from the pressure value. Elsewhere, the internal pressure effects are examined through the magnetic and photomagnetic investigations on powders of the solid-solutions based on the Mn ion, $[Fe_xMn_{1-x}(PM\text{-}PEA)_2(NCS)_2]$. Growing the Mn ratio increases the internal pressure, allowing to control the hysteresis width and the paramagnetic residue but also to enhance the efficiency of the photo-induced SCO. The comparison of the quenching and light-induced behaviors reveals a complex phase-diagram governed by internal pressure, temperature and light.

Keywords: spin crossover (SCO); pressure; metal-coordination chemistry; light-induced SCO; crystallography; metastable state; iron; solid solution

1. Introduction

The use of pressure to perturb the electronic structure and the physical properties of metal-coordination compounds is an interesting way for the search towards switching materials [1]. The role of pressure has been studied for many years on spin crossover (SCO) compounds since it has applications in many fields as diverse as biology [2–4], geology [5,6], physics and chemistry [7–10]. The pressure-induced SCO opens the corresponding materials to many potential applications, including piezo-chromism [11].

The SCO materials usually contract under the application of an external pressure since the latter favors the diamagnetic low-spin (LS), state which has a lower volume than the paramagnetic high-spin (HS) state. This is due to the occupation by electrons of anti-bonding molecular orbitals in HS that increases the iron(II)-ligand bond lengths in contrast to the non-bonding molecular orbitals occupied by electrons in LS. Consequently, the expected straightforward pressure-induced modifications of the

thermal SCO features are an increase of the SCO temperatures and of the LS residues together with a decrease in the sharpness of the transition. These features are confirmed by considerations based on thermodynamics and theoretical models [8–10,12–14] that also predict some interesting consequences such as the decrease of the hysteresis width with increasing pressure. From the experimental point of view, many counter-examples have been reported so far [15]. For example, non-expected hysteresis broadening [16] as well as irreversible behaviors were reported for some compounds [10,17]. Even in a family of very similar complexes, a variety of high pressure behaviors can be observed. This is the case of the $[Fe(PM\text{-}L)_2(NCS)_2]$ family (with PM-L = *N*-(2′-pyridylmethylene)-4-(aromatic function L)), showing that expectations can be fulfilled, or not, depending on the nature of the L part of the ligand [15,18]. Furthermore, in some cases, the application of pressure on a SCO material can even favor the HS state. This non-intuitive behavior was observed in Mössbauer studies in mononuclear phenanthroline [19] or poly(1-pyrazol)borate [20] iron(II) complexes, and was also reported for the two-dimensional compound $[Fe(btr)_2(NCS)_2]\cdot H_2O$ (btr = 4,4′-bis-(1,2,4-triazole)) [21]. As a general matter, the number of discrepancies between expectations and experiments deserves a further investigation of the application of an external pressure on SCO materials. The concept of external pressure must be understood in a large view since it should include *ex situ* and *in situ* situations; taking in mind that SCO molecular materials are sensitive to a pressure range weaker than the one used in solid-state chemistry. The first part of this work is dedicated to such approach.

Elsewhere, another way to induce a pressure on the SCO molecule within the material is to synthetize solid-solutions mixing the iron(II) spin-transition compound and an isostructural compound; the latter being based on a metal-ion having no spin transition. This method refers therefore to a so-called internal pressure. In such a case, depending on the volume of this metal ion in comparison to that of the iron(II) ion, the substitution will act as a pressure or a negative pressure factor. Solid-solution investigations have been conducted since the 1970s on SCO complexes of iron(II) and iron(III) using a large variety of diluting ions. The size of the latter increases from Ni(II), Zn(II), Co(II), Mn(II) to Cd(II). The general tendencies observed upon metal dilution are (i) a more and more gradual spin crossover with increasing doping ratio because of the weakening of cooperativity; (ii) a lowering of the equilibrium temperature $T_{1/2}$ more effective when the doping ion volume is important and (iii) a potential appearance of LS fraction at high temperature, or HS fraction at low temperature [22–29]. Regarding the decrease of the temperature of transition, the assumptions are based essentially on the concept of internal pressure, *i.e.*, the relative sizes of the metal ions. A doping metal ion, having no spin transition, corresponds to a unit-cell volume that is different from the one obtained with the iron ion. In the solid-solution, the bigger the doping ion, the larger the unit-cell and the larger is the volume available for the iron-ion within the crystal packing. Consequently, large unit-cells favor the state of larger volume of the iron(II), therefore the HS state. Accordingly, the temperatures $T_{1/2}$ are shifted to low temperatures when large metal ions are used to dope the SCO material; HS residue being also favored.

The effect of internal pressure on light-induced spin-state lifetime has been mainly reported by A. Hauser [30–32]. The lifetime of the metastable HS state reached by LIESST effect (Light-Induced Excited Spin-State Trapping) [33] has been extensively studied to evidence that its relaxation is governed by tunneling effect at low temperature and therefore temperature independent in this region. In contrast, at higher temperature, the relaxation is governed by a thermally activated process. The studies on solid solutions have demonstrated that the relaxation of the photo-induced metastable HS state of the iron(II) is weakly influenced by a small metal dilution in the thermally activated region while it is strongly accelerated in the tunneling region. This has also been evidenced by a systematic investigation of the T(LIESST) temperature that records the temperature range of observation of the HS metastable state. T(LIESST) is obtained by the inflexion point position of the derivative of the $\chi_M T$ *vs* T plot (χ_M stands for the molar magnetic susceptibility) recorded after light irradiation [34–36]. This temperature, obtained after warming at a given temperature scan rate, was shown to be constant [28,29,37,38] or slightly increased [39–41] upon metal dilution.

In this article, we report the effects of internal and external pressure on the strongly cooperative compound [Fe(PM-PEA)$_2$(NCS)$_2$] (with PM-PEA = *N*-(2′-pyridylmethylene)-4-(phenylethynyl) aniline). This compound has been described in 1997 [42] and shows a spin transition with a large hysteresis loop between 190 K and 232 K when measured on powder and between 215 K and 234 K when measured on single crystals [43]. This hysteresis is accompanied by a phase transition between a monoclinic $P2_1/c$ space group in the HS state and an orthorhombic *Pccn* space group in the LS state. The crystal structure of the thermal quenched HS phase at 30 K is similar to the $P2_1/c$ phase at room temperature. Regarding the photomagnetic properties, the LIESST effect remains poorly efficient. A first magnetic study under external pressure was performed in 1998 [18] revealing a shift of the thermal hysteresis towards low temperature and an irreversible effect of pressure. This compound deserves a more detailed investigation, both on the structural behavior under external pressure and on the effect of internal pressure on the thermal and light-induced spin transition. This paper first describes the effect of *in situ* and *ex situ* external pressures from a crystallographic point of view. Subsequently, the magnetic behavior of the [Fe$_x$Mn$_{1-x}$(PM-PEA)$_2$(NCS)$_2$] solid-solution allows to examine the effects of an internal pressure; the thermally quenched and the light-induced HS states being also explored.

2. Results and Discussion

2.1. External Pressure on [Fe(PM-PEA)$_2$(NCS)$_2$]

Early studies on the effects of applying a pressure on [Fe(PM-PEA)$_2$(NCS)$_2$] clearly indicated from magnetic measurements that the hysteresis loop is affected in an irreversible mode using a relatively weak pressure [18]. The hysteresis width looked indeed enlarged by a few degrees after that a pressure inferior to 300 MPa was applied to the material. The release of the pressure did not correspond to a return to the initial SCO properties; the broadening of the hysteresis being conserved. However, as a general matter, clear evidence for noticeable effects on the SCO properties of *ex situ* pressure has been rarely reported so far. This feature is probably a path that has been underestimated in the SCO materials study despite it may open this research field to new applications or simply to new solid-state phases and properties [44]. It is worth defining what is called *ex situ* pressure; that is the situation when pressure has been applied on the sample, then released so as the physical measurements take place at ambient pressure (0.1 MPa).

The purpose of the present work was to confirm possible *ex situ* effects on the SCO features of the investigated compound. Because of the discrepancy of SCO properties shown by this compound when looking at different synthesis and different sample forms and diverse techniques [45], we decided to work only on single crystals coming from the same synthesis batch and to investigate the pressure effects with the same method, here X-Ray Diffraction (XRD). Note that this discrepancy has been notably attributed to the possible presence of defects, such as methanol inclusions at variable ratio for instance.

2.1.1. SCO at High-Pressure

Before investigating the consequence of *ex situ* pressure, we checked the effect of *in situ* pressure mainly to detect if this compound could show a SCO at room temperature under pressure. Some compounds of the same series have shown a SCO at room temperature but for pressure higher than 700 MPa [46,47]. Let us recall that single crystals of [Fe(PM-PEA)$_2$(NCS)$_2$] are well-known from variable temperature measurements [43] to crystallize in the monoclinic system in the HS state and in the orthorhombic system in the LS state; the unit-cell volume variation due to the thermal SCO being of the order of 3%. Note that this value corresponds to a small amplitude of the contraction-expansion process [44] which masks a strong anisotropy. In fact, the *a* unit-cell parameter strongly contracts (−9%) while the *c* parameter increases (+4%) at the SCO. One of the consequences of the structural modifications is that single-crystals are most of the time strongly damaged by the SCO.

The unit cell parameters were determined under *in situ* pressure in the range 60 MPa to 1135 MPa (Table 1). From 60 to 365 MPa there is a contraction of the unit-cell corresponding to about 5% of the initial volume following a regular variation of 0.54 Å^3/MPa. At higher pressure, there is a modification of the crystal system, from monoclinic to orthorhombic concomitant with a sharp fall of the unit-cell volume by 4.3% between 365 and 465 MPa; therefore a modification of 1.57 Å^3/MPa. The decrease of the volume corresponds to a strongly anisotropic change of the unit-cell parameters with a noteworthy decrease of *a* (−8%) and an increase of *c* (+4.8%). These modifications can be without a doubt attributed to the HS to LS conversion in this compound from the similitude with the thermal SCO. The alteration of the crystal quality at 465 MPa and above reinforces such conclusion. Consequently, [Fe(PM-PEA)$_2$(NCS)$_2$] undergoes a SCO under a pressure of about 400 MPa. This compound appears therefore one of the molecular material showing a room-temperature SCO under the lowest pressure value.

Table 1. Unit-cell parameters and volume as a function of the *in situ* pressure (1 MPa = 10 bars) determined by X-ray diffraction using diamond anvil cells for a [Fe(PM-PEA)$_2$(NCS)$_2$] single-crystal. The calculated standard deviations are of the order of magnitude of 0.005 Å on lengths, 1 Å^3 on the volume and 0.02° on angles.

***In situ* Pressure (MPa)**	***a* (Å)**	***b* (Å)**	***c* (Å)**	**β**	***V* (Å^3)**	**Crystal System**
60	15.659	14.482	16.844	93.00	3814	monoclinic
150	15.624	14.315	16.746	92.97	3740	monoclinic
248	15.621	14.116	16.716	92.94	3681	monoclinic
365	15.605	13.968	16.622	92.81	3619	monoclinic
465	14.356	13.850	17.415	90	3462	orthorhombic
658	14.147	14.147	17.119	90	3426	orthorhombic
1135	14.099	13.687	17.032	90	3287	orthorhombic

In order to proceed to the fine analysis of the structural properties of the pressure-induced SCO, the determination of the crystal structure at high pressure is mandatory. Unfortunately, the strong alteration of the crystal quality has forbidden such approach. One full data collection in the HS state was however performed at 55 MPa and the results are used below.

2.1.2. *Ex situ* Pressure Effects

The study of the irreversible effects of applying a pressure on [Fe(PM-PEA)$_2$(NCS)$_2$] is performed also on single-crystals. The latter were taken from the synthesis batch and the pressure applied for a few minutes before being released. The XRD experiment is then performed at atmospheric pressure. A fresh crystal is taken at each pressure investigation. Since pressures higher than 400 MPa induce a SCO that strongly damage the sample and since the aim is to investigate weak pressure effects, the study was limited to pressure lower than 200 MPa. For each sample, a full XRD data collection was run after the release of the pressure at room temperature and, in addition, a temperature dependence study of the unit-cell parameters was performed to track the thermal SCO. Investigations were performed pressures (MPa) of 0.1 (ambient pressure), 20, 80, 110 and 200 as well as 0.001 that corresponded to putting the sample under vacuum. The 0.1 and 20 MPa experiments were performed on the same crystal. Table 2 reports the main features of the crystal-structure determinations with in addition those of the above *in situ* study.

The unit-cell parameters variation as a function of temperature is an efficient tool to visualize the thermal SCO. The comparison of this variation for a single crystal that has not been submitted to pressure (0.1 MPa) with the variation for a single crystal that was previously submitted to 20 MPa is shown on Figure 1. Remarkably, the SCO features appear completely modified by the pressure treatment. The temperature of SCO are strongly translated to lower temperatures with a more pronounced effect for $T_{1/2\text{down}}$ resulting in a colossal increase of the hysteresis width from 19 K to 63

K. The same procedure is applied for various *ex situ* pressure and the SCO temperatures are reported in Table 3. The same behavior is observed in each case resulting in an increase of the hysteresis that is apparently not dependent on the value of the applied pressure. Even the use of a negative pressure (0.001 MPa) gives the same conclusions. Consequently, changing once the pressure on the sample strongly enlarges the hysteresis width. This pressure effect is not reversible (at least for a few weeks) and looks independent from the pressure-value.

Table 2. Selected experimental and structural parameters from the full X-Ray Diffraction data collections at room temperature for single crystals of $[Fe(PM\text{-}PEA)_2(NCS)_2]$ under diverse pressure conditions. The Root Mean Square Deviations (RMSD) with the reference crystal structure of the compound are given.

Pressure (MPa)	**55 *in situ***	**20 *ex situ***	**80 *ex situ***	**110 *ex situ***	**200 *ex situ***	**0.001 *ex situ***
a (Å)	15.652(5)	15.653(1)	15.668(1)	15.688(5)	15.6600(6)	15.645(1)
b (Å)	14.434(4)	14.523(1)	14.571(1)	14.521(5)	14.5380(8)	14.555(1)
c (Å)	16.785(3)	16.825(1)	16.869(1)	16.841(5)	16.8252(9)	16.863(1)
β (°)	93.053(7)	93.011(4)	93.114(5)	93.163(5)	93.066(3)	93.161(5)
V (Å^3)	3786(2)	3819.9(5)	3845.6(4)	3831(2)	3825.0(3)	3834.3(6)
Refl. coll.	11749	25950	15716	10769	25950	21614
Refl. obs. (I > 2σ)	2441	3286	3214	2411	3286	4457
*R*int	0.081	0.138	0.071	0.063	0.139	0.058
*R*obs (all)	0.058(0.192)	0.058(0.111)	0.043(0.086)	0.052(0.101)	0.075(0.223)	0.054(0.115)
w*R*2obs (all)	0.103(0.136)	0.162(0.226)	0.095(0.111)	0.089(0.111)	0.162(0.226)	0.112(0.143)
RMSD	0.0353	0.0299	0.0320	0.0337	0.0318	0.0312

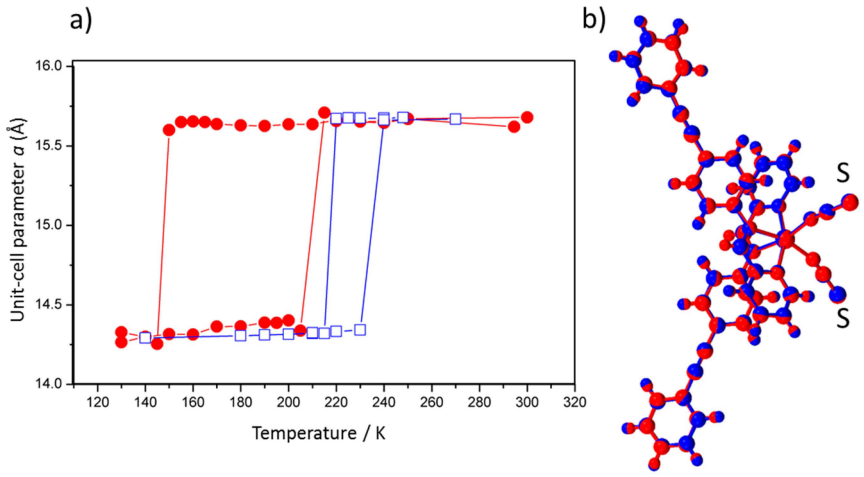

Figure 1. (**a**) Temperature dependence of the unit-cell parameter *a* for $[Fe(PM\text{-}PEA)_2(NCS)_2]$ for a crystal as-synthesized (empty blue square) and after the crystal was submitted to a pressure of 20 MPa (filled red circle) and (**b**) views of the superposition of the molecular structure before (blue) and after (red) application of a pressure of 20 MPa.

Table 3. Spin-Crossover features for $[Fe(PM\text{-}PEA)_2(NCS)_2]$ as a function of pressure applied *ex situ*. The SCO temperatures ($T_{1/2}\downarrow$ and $T_{1/2}\uparrow$) and the hysteresis width (ΔT) come from single-crystal XRD measurements at variable temperatures by analogy with the result presented in Figure 1. The experimental temperature-accuracy is estimated to 2 K.

***Ex situ* Pressure (MPa)**	**0.1 (Ambient)**	**20**	**80**	**110**	**200**	**0.001 (Vacuum)**
$T_{1/2}\downarrow$ (K)	216	150	163	165	161	175
$T_{1/2}\uparrow$ (K)	235	213	215	225	213	218
ΔT (K)	19	63	52	60	52	43

The increase of the hysteresis width shown here on $[Fe(PM\text{-}PEA)_2(NCS)_2]$ confirms the irreversible effects of pressure already anticipated from magnetic measurements [18]. A fine comparison of both cases is hardly applicable due to the differences in experimental protocols and techniques. Note that a similar behavior was observed on a quite different SCO compound, $[Fe(sal_2\text{-}trien)][Ni(dmit)_2]$, where the application of 50 MPa induced a very large increase of the hysteresis width together with signs for an irreversible feature of these modifications [17]. Even though never clearly evidenced; other signs of irreversible effects of pressure were suspected in previous studies of SCO materials [10,19,48].

In the scrutiny of the structure-properties relationship of the $[Fe(PM\text{-}L)_2(NCS)_2]$ complexes, it was demonstrated that the SCO temperatures are mostly linked to the shortest S...C intermolecular distance between the sulfur atom of the NCS branch and the closest carbon atom of the neighboring molecule [49,50].

In the present case, this S...C distance is almost identical in all the crystal-packings since it is measured at 3.463(9) Å for the reference sample and is in the range [3.457(6)–3.475(8) Å] for all the determined crystal structures of the pressurized samples. Taking into account the standard deviations, there are therefore no noticeable differences induced by pressure on this crucial structural feature. Furthermore, a superimposition of the atomic positions (Figure 1) shows no obvious structural change with pressure as also illustrated by the small Root Mean Square Deviations (RMSD) between the initial crystal structure and the ones determined in this work (Table 2). A small difference can only be noted, even though at the limit of the resolution. It concerns the intramolecular S...S distance that is at 7.384(2) Å at 20 MPa and higher pressures while it is at 7.359(2) Å for the reference (Figure 1). This distance increases to 7.395(2) Å at 0.001 MPa. This change on the S atom positions could be the visible mark of a global but very subtle ordering of the crystal structure, not perceptible with the present results. As a general matter, the possible influence of very small change of structural properties on SCO features is well demonstrated, including hysteresis width [44,51,52]. Another hypothesis is that the modifications of the SCO features observed here but not explain from the crystal-structures examination could be related to another physical scale, which is the microstructural one. The latter refers to coherent domains features and microstrains, not investigated here.

In any case, the pressure effect observed here should push to more systematic investigations of *ex situ* pressure effects on SCO materials.

2.2. Internal Pressure

2.2.1. Synthesis

The synthesis of the $[Fe_xMn_{1-x}(PM\text{-}PEA)_2(NCS)_2]$ complexes was adapted from the previously described method [42]. No single-crystals of the solid solutions could have been obtained. The compositions of the crystalline powders were determined by chemical analysis (see experimental section) as x = 1 (1), x = 0.90 (2), x = 0.85 (3), x = 0.79 (4), x = 0.73 (5), x = 0.68 (6), x = 0.56 (7), x = 0.48 (8), x = 0.36 (9) and x = 0 (10). X-ray powder diffractograms were recorded for each solid solution (Figures S1 and S2) revealing that 1–10 are isomorphs and adopt the crystal structure already reported for 1 that was determined from single-crystals [42,43]. The powder diffractograms were analyzed using the Le Bail method [53]. The unit-cell parameters dependence as a function of the Fe/Mn ratio is reported in Table S1 of the Supplementary Information.

2.2.2. Magnetic Properties

Magnetic measurements were performed on the ten powder samples labelled from 1 to 10. Figure 2 reports the temperature dependence of the HS fraction γ_{HS} that was extracted from equations 1 and 2 for 1–9. This allows to remove the contribution of the paramagnetic manganese(II) ion (d^5, $S = 5/2$).

$$\chi_M T = x(\chi_M T)_{Fe} + (1-x)(\chi_M T)_{Mn} \quad (1)$$

$$\gamma_{HS} = (\chi_M T)_{Fe}/(\chi_M T)_{Fe(T\,=\,300K)} \quad (2)$$

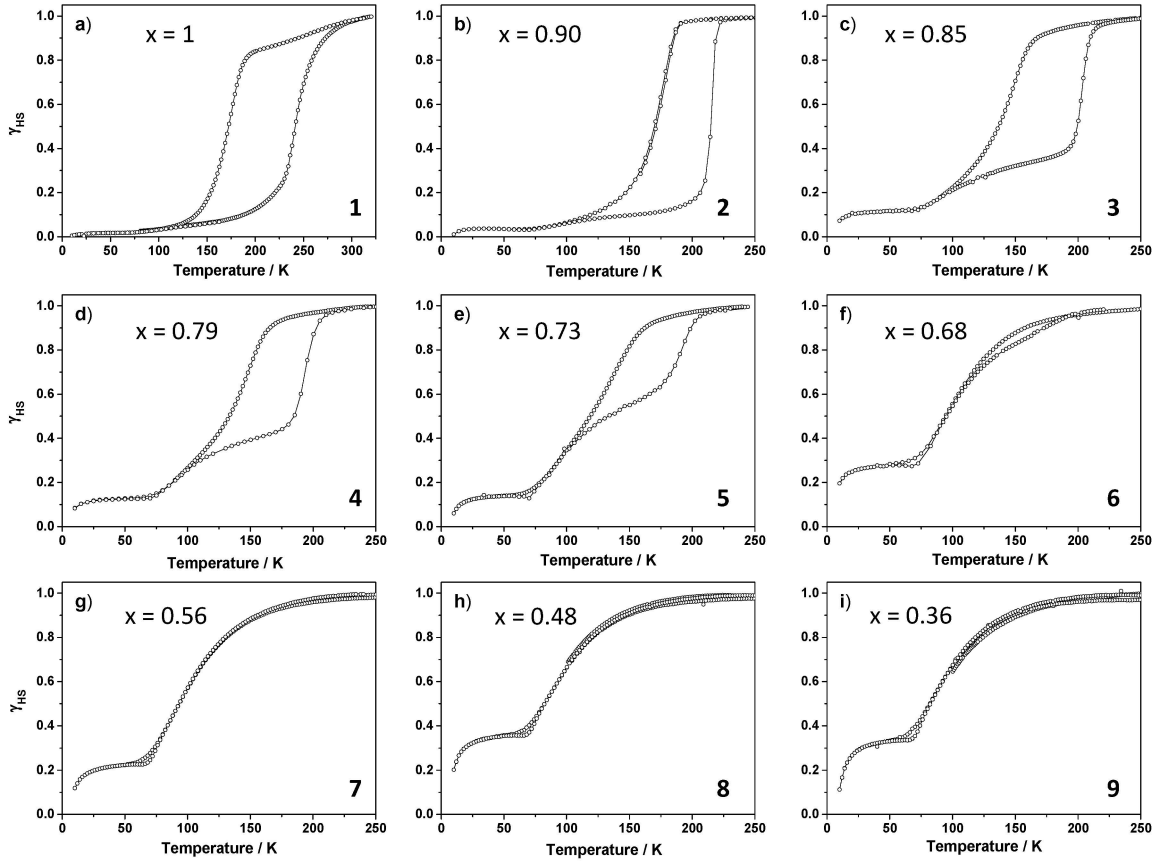

Figure 2. Thermal behavior of the high spin fraction, γ_{HS}, for the different solid solutions $[Fe_xMn_{(1-x)}(PM\text{-}PEA)_2(NCS)_2]$ (**a**) 1 ($x = 1$), (**b**) 2 ($x = 0.90$), (**c**) 3 ($x = 0.85$), (**d**) 4 ($x = 0.79$), (**e**) 5 ($x = 0.73$), (**f**) 6 ($x = 0.68$), (**g**) 7 ($x = 0.56$), (**h**) 8 ($x = 0.48$), (**i**) 9 ($x = 0.36$).

As already reported [42] and described above, compound 1 exhibits a complete spin-crossover. In the present experimental conditions, the SCO temperatures are $T_{1/2}(\downarrow)$ = 170 K and $T_{1/2}(\uparrow)$ = 245 K, defining a large hysteresis loop, 75 K wide, which is larger than the previously reported values. This underlines the role of crystallinity in spin-crossover which can affect the conversion properties. As mentioned in part 2.1 of the present paper, small differences in crystalline quality are known to affect the SCO temperatures for this sample; which probably comes from the presence of defects [43,45]. The differences of SCO temperatures in comparison with those presented in the above discussion on external pressure probably come from the fact the latter were performed on samples in the form of single-crystals.

Here, upon metal dilution from 1 to 9, (i) the hysteresis tends to disappear and (ii) to shift to low temperature with (iii) a paramagnetic residue appearing at low temperature. Below 50 K, the spin states are frozen but the $(\chi_M T)_{Fe}$ contributions exhibit a typical decrease assigned to the zero-field-splitting effect of HS iron(II) ions. This contribution is hard to quantify and was not removed to plot the γ_{HS} fraction. The derived temperature data are listed in Table 4. Note that, the clear assignment of the transition temperature for 4–9 becomes risky since the spin conversion is not complete and very gradual. These values have been estimated at half of the transiting HS fraction. On the basis of this estimation, it appears that the warming branch is more significantly affected by the metal dilution than the cooling one. From 1 to 9, $T_{1/2}\uparrow$ decreases by 147 K while $T_{1/2}\downarrow$ only decreases by 72 K. This last shift could be underestimated due to an incomplete SCO.

Table 4. Summary of the experimental data from the magnetic study of $[Fe_xMn_{1-x}(PM\text{-}PEA)_2(NCS)_2]$.

Compound	x	$T_{1/2}\uparrow$ (K)	$T_{1/2}\downarrow$ (K)	ΔT (K)	T(LIESST) (K)	T(TIESST) (K)
1	1	245	170	75	65	66
2	0.90	218	160	58	65	67
3	0.85	202	141	61	66	67
4	0.79	191	137	54	65	66
5	0.73	190	134	56	65	66
6	0.68	108	108	-	67	66
7	0.56	105	105	-	67	67
8	0.48	100	100	-	67	67
9	0.36	98	98	-	67	66
10	0	-	-	-	-	-

In previous works [39–41], we have shown that an increase of the low-temperature residual HS fraction may originate from static and kinetic effects. The static effect comes from the negative internal pressure generated by the Mn(II) ions in the Fe(II) SC matrix. Indeed the ionic radius decreases in the following order: r (Mn^{2+}) (r = 83 pm) > r (Fe_{HS}^{2+}) (78 pm) > r (Fe_{LS}^{2+}) (61 pm) [54]. The negative internal pressure stabilizes the HS state which has a larger volume than the LS state and may lead to a stable paramagnetic (HS) residue at low temperature [22–29]. The kinetic effect corresponds to an increase of the lifetime of the metastable state, which may be quenched at low temperature and gives rise to an alteration of the hysteresis loops due to the overlap between the T(LIESST) and the hysteresis curves [39–41]. This alteration cannot be seen in the 1–9 compounds either because the loss of hysteresis occurs before the overlap with the T(LIESST) or by the absence of any kinetic effect.

Another unusual aspect of these experimental curves is the occurrence of a two-step SCO in the warming branch of the hysteresis in 3–5. The first step is gradual and is superimposed on the cooling branch. Upon further warming, an intermediate plateau appears; opening the hysteresis loop. This particular feature could come from the phase transition occurring in the pure iron compounds that concerns less and less amount of domains in the powder when the dilution is increasing. Indeed between 1 and 2, there is a reduction of the hysteresis width from 75 K to 60 K while from 2 to 5, this width does not change but, the HS fraction involved in this hysteresis is decreasing and disappears in 6. One hypothesis to explain these two steps is the presence of two different phases for the LS state leading to two different SCO; one which exhibits the orthorhombic to monoclinic phase transition associated to the hysteresis loop; one which does not present this phase transition and exhibit a gradual spin conversion. This second type leads to gradual SCO and could correspond to the iron(II) located around the manganese(II) ions which act as defects in the crystal packing.

2.2.3. T(LIESST) and T(TIESST) *versus* Internal Pressure

The metastable state has been investigated by light irradiation and fast cooling of the HS phase. The LIESST effect was obtained by irradiating the sample at 10 K at 830 nm, which is the most efficient wavelength for this compound. Once the photostationary point reached, the light was switched off and the temperature was increased at 0.4 K/min to record the T(LIESST) temperature [34–36]. The same procedure is followed after fast cooling of the high-temperature phase that led to the Thermally-Induced Excited Spin-State Trapping (TIESST). The T(LIESST) and T(TIESST) values are obtained by the minimum in the derivative of theses curves.

Figure 3 reports the experiments performed on 1–9 and Table 4 reports the T(LIESST) and T(TIESST) temperatures. The first observation is that upon metal dilution, the LIESST effect becomes more efficient by 20% in 1 and up to a complete photoswitching in 6–9. This increase of efficiency could follow from the loss of cooperativity and probably the loss of phase transition as discussed above. Indeed, in the pure iron compound, cooperativity is so important, that the rigidity of the structure could avoid an efficient light conversion by disfavoring the propagation of the inherent volume change upon LS → HS conversion. Since the metal dilution effect is first to weaken the cooperativity

and secondly to favor the HS state through the internal pressure applied by the manganese ions, these two effects should favor the efficiency of the light excitation. Another origin of this improved photo-conversion could be that the introduction of manganese ion reduces the strong Metal-Ligand Charge Transfer band of the compound, allowing light to penetrate into the sample more efficiently and therefore increasing the photo-switching.

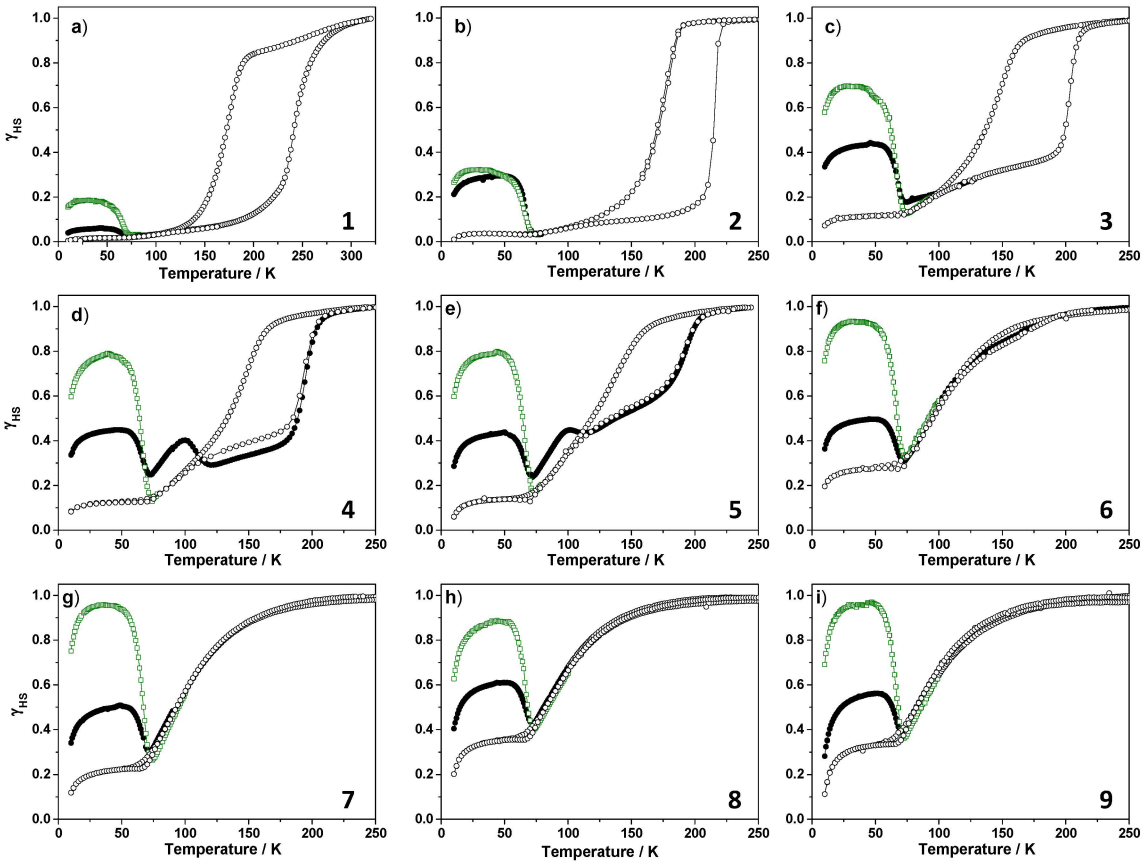

Figure 3. Thermal behavior of the HS fraction, γ_{HS}, of the different solid-solutions $[Fe_xMn_{(1-x)}(PM\text{-}PEA)_2(NCS)_2]$ upon slow cooling and warming (o), after fast cooling from room temperature to 10 K (•) and after irradiation at 830 nm of the slowly cooled phase (□) for (**a**) 1 (x = 1), (**b**) 2 (x = 0.90), (**c**) 3 (x = 0.85), (**d**) 4 (x = 0.79), (**e**) 5 (x = 0.73), (**f**) 6 (x = 0.68), (**g**) 7 (x = 0.56), (**h**) 8 (x = 0.48), (**i**) 9 (x = 0.36).

This observation contrasts with the TIESST effect whose efficiency increases from 1 (8%) to 3 (30%) but remains at this level upon further metal dilution. This is probably due to the experiment that is only a fast cooling from 300 K to 10 K and not an instant quench, which strongly differs from the thermal-quenching previously performed on an X-Ray diffractometer, showing similar structures between the high temperature and the metastable HS phases [55]. Note that the discrepancy between magnetic and diffraction experiments in term of quenching effect investigation were discussed elsewhere on a similar material [56]. This effect remains however quite surprising since the efficiency of thermal quenching is expected to increase with the decrease of $T_{1/2}$.

Furthermore, the T(LIESST) and T(TIESST) values are not affected by the insertion of manganese in the structure. This behavior has already been reported on $[Fe_xM_{1-x}(phen)_2(NCS)_2]$ and $[Fe_xM_{1-x}(bpp)_2](NCS)_2$ [28,37] and has been interpreted as a clear illustration that the T(LIESST) is of molecular origin and is almost independent on the collective character of the compound; this assumption being demonstrated elsewhere [44]. Similarly to these previous works, the apparition of the HS residue at low temperature occurs below 75 K which corresponds to the end of the T(LIESST)

and *T*(TIESST) curves. The stability of this residue has been tested by relaxation kinetics. The magnetic signal remains constant and no relaxation could have been observed. This residue is either only due to the effect of internal pressure following the metal dilution or to the low value of $T_{1/2}$ leading to a freezing of the HS fraction.

Finally, the most surprising feature of the curves reported in Figure 3 is the *T*(TIESST) curves of 3–5. During the warming that follows the fast cooling, the HS fraction firstly decreases and the *T*(TIESST) value is measured, and upon further warming the HS fraction is stable (3) or increases up to a maximum at 100 K (4 and 5). After this maximum, the HS fraction decreases and reaches the warming branch of the hysteresis loop, especially in 5. The fact that this phenomenon is not observed in the *T*(LIESST) curves is in favor of a phase transition occurring during the warming. The crystal structure of the photo-induced phase is unknown while the thermally quenched state, HS_1*, has the same crystal structure than the HS phase at room temperature, HS_1. The photo-induced HS state is obtained from the LS state, labelled LS_2, which has a different crystal arrangement from the HS_1 and HS_1* ones. This so called HS_2* state has probably the same structure than the LS_2. In the case of the HS thermally quenched state, HS_1*, its relaxation with temperature probably competes with the structural $P2_1/c$–$Pccn$ phase transition. In other words, these considerations reveal a complex interplay between structural phases and spin state in this compound. A deeper investigation of the metastable state is performed below with the aim to propose an overview of the phase diagram.

2.2.4. Focus on the Thermally-Quenched Metastable-State

The thermally-quenched metastable-state has been deeper investigated, especially for compounds 3–5. The behavior of compound 4 has been measured again on a freshly synthesized sample. Figure 4 reports The *T*(TIESST) curve followed by the warming branch of the hysteresis. The maximum observed around 95 K is recovered. Upon cycling, the further fast thermal cooling drastically changed the shape of the *T*(TIESST) curves where the maximum at 95 K is strongly reduced in intensity from 40% to 30% of the HS fraction. This result demonstrates a change associated with the first cooling/heating cycle without any further changes during the next cycles.

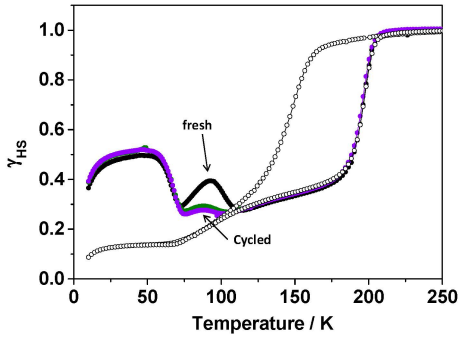

Figure 4. Thermal behavior of the HS fraction, γ_{HS}, of a fresh sample of 4 ($[Fe_{0.79}Mn_{0.21}(PM\text{-}PEA)_2(NCS)_2]$), upon slow cooling and warming (o), after first fast cooling from room temperature to 10 K (•) and after further fast cooling processes (• and •).

Based on the different results we can propose a phase diagram to locate the different phases (Figure 5). At high temperature, the material is in its monoclinic HS_1 structure. Slow cooling brings the material into the orthorhombic LS_2 state which is converted back in the HS_1 state upon warming to room temperature. However, the presence of a stepped warming branch of the hysteresis of 3–5 indicates that at low temperature, two kind of LS states are present. LS_2 should be the one exhibiting the crystallographic change being responsible of the hysteretic part of the curve. The low temperature part of the transition, the one which does not exhibit any hysteresis could follow from the absence of any phase transition and therefore a $LS_1 \rightarrow HS_1$ conversion.

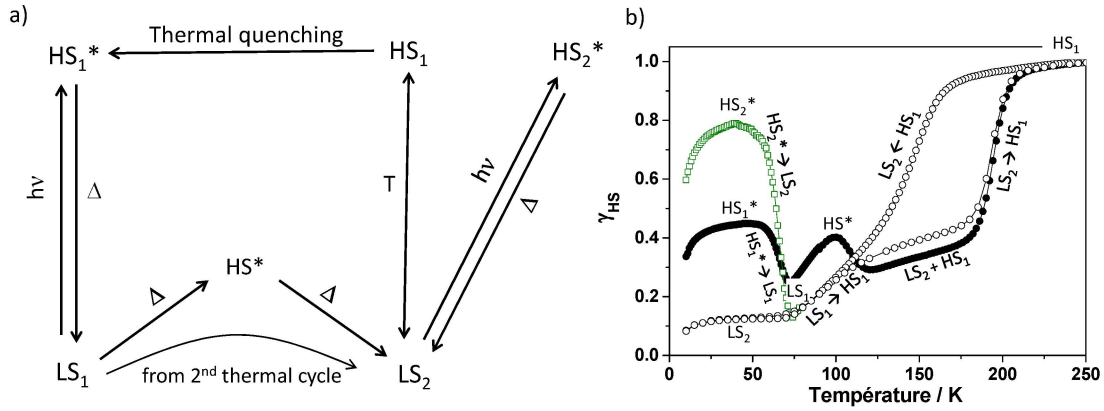

Figure 5. Tentative summary of the spin-state phase-diagram (**a**) of the compounds $[Fe_xMn_{1-x}(PM\text{-}PEA)_2(NCS)_2]$ ($0.85 < x < 0.70$) from magnetic and photo-magnetic measurements (**b**). HS_1 and HS_1* crystallize in the monoclinic crystal system and LS_2 crystallizes in the orthorhombic one. Label 1 refers to the monoclinic phase and label 2 to the orthorhombic phase.

Rapid cooling keeps the material in its HS_1 metastable phase (denoted HS_1*). Upon slow warming (0.4 K/min) this phase relaxes toward LS_1, from which a new HS metastable state, HS*, is reached by further warming (Figure 5). By heating above 90 K, this new HS* state relaxes to the LS_2 and further to the HS_1 state. In the second cycle, a new relaxation path is accessible, shortcutting the appearance of the HS* state. This HS* phase is slightly hidden along this second relaxation path. This could be due to a loss of crystallinity upon thermal cycling. One hypothesis is that HS* could be the resultant of the $LS_1 \rightarrow HS_1$ conversion that occurs in the 70–90 K range and the relaxation of the remaining HS_1* that could have been stabilized by the $LS_1 \rightarrow HS_1$ conversion. Upon warming above 90 K, the remaining HS_1* would relax to the LS_2 state.

A subsequent experiment was conducted to compare the photo-induced behavior of the HS state reached by irradiation from the LS_2 and the LS_1 states. Figure 6 reports the T(LIESST) curve of the HS state obtained from LS_2 (green curve). The following T(LIESST) curve recovers the spin-crossover curve and the hysteresis above 60 K. No further bump in the curve was observed. On a fresh sample, we have quickly cooled the sample to 10 K to reach the HS_1*. The temperature was increased up to 71 K (corresponding to the minimum of the curve T(TIESST)), and then quickly cooled down to 10 K. The sample was then irradiated and the HS fraction reached almost 80%, indicating a better efficiency than from the LS_2 state. Once reached the photo-stationary state, the irradiation was switched off and the temperature increased at the rate of 0.4 K/min (Figure 6). The T(LIESST) curve exhibits a first decrease around 65 K, similarly to the first T(LIESST) from the LS_2 state. Upon further warming, a small bump is observed with a maximum at 90 K, corresponding to the HS* state. It seems that from irradiating the LS_2 state, the HS state reached, HS_2*, is different from HS_1* obtained from LS_1. While HS_2* relaxes directly to the LS_2 state, HS_1* relaxes first to LS_1 and then to LS_2, going through the intermediate HS* (Figure 5).

This particular shape of the T(LIESST) curve is rarely reported in the literature. One similar shape of T(LIESST) was however described in 2009 on a binuclear compound. This behavior has been explained by a competition between the different states of the binuclear that are HS-HS, HS-LS and LS-LS [56]. Analogy with such conclusions might be performed here due to the presence of two different metallic sites within the materials, those of Fe that can undergo a SCO and those of Mn that do not.

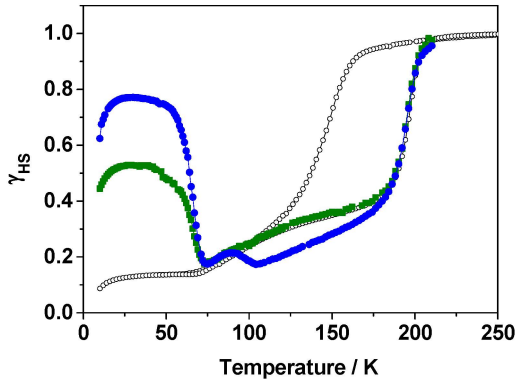

Figure 6. Thermal behavior of the HS fraction, γ_{HS}, of a fresh sample of 4 (x = 0,79), upon slow cooling and warming (o), after first irradiation of the slowly cooled phase at 10 K (•) and after irradiation at 10 K of the quickly cooled state previously relaxed at 70 K (•).

3. Experimental Section

The synthesis of the PM-PEA (PM-PEA = *N*-(2′-pyridylmethylene)-4-(phenylethynyl)aniline) ligand followed the procedure previously reported [42]. The synthesis of the $[Fe_xMn_{1-x}(PM\text{-}PEA)_2(NCS)_2]$ solid solutions followed the procedure described in [42] by mixing the appropriate amount of iron(II) sulfate and manganese(II) chloride. The composition of compounds 1–9 was determined by elementary chemical analysis and CAMECA SX 100 microprobe-electron beam technique (CAMECA SAS, Gennevilliers, France). Unsuccessful mineralization prevented ICP-OES analysis, of Fe and Mn cations. Scans over 3000 μm^2 by microprobe technique evidenced homogeneous samples with no segregation of either metal and co-precipitation of KCl. Precise values of x were determined for 1 (x = 1), 2 (x = 0.90), 3 (x = 0.85), 4 (x = 0.79), 5 (x = 0.73), 6 (x = 0.68), 7 (x = 0.56), 8 (x = 0.48) and 9 (x = 0.36). Elemental Anal (%) Calc. for compound 1 $[Fe(PM\text{-}PEA)_2(NCS)_2]$ C 68.48, H 3.83, N 11.41, S 8.71. Found C 67.07, H 3.79, N 11.19, S 8.78. Calc. for Compound 2 $[Fe_{0,902}Mn_{0,098}(PM\text{-}PEA)_2(NCS)_2]$ C 68.48, H 3.83, N 11.41, S 8.71. Found C 66.82, H 3.84, N 11.19, S 8.87. Calc. for Compound 3 $[Fe_{0,848}Mn_{0,152}(PM\text{-}PEA)_2(NCS)_2]$ C 68.49, H 3.83, N 11.41, S 8.71. Found C 67.60, H 3.81, N 11.10, S 8.72. Calc. for Compound 4 $[Fe_{0,788}Mn_{0,212}(PM\text{-}PEA)_2(NCS)_2]$ C 68.50, H 3.83, N 11.41, S 8.71. Found C 67.12, H 3.79, N 11.17, S 8.81. Calc. for Compound 5 $[Fe_{0,733}Mn_{0,267}(PM\text{-}PEA)_2(NCS)_2]$ C 68.51, H 3.83, N 11.41, S 8.71. Found C 66.90, H 3.86, N 11.12, S 7.15. Calc. for Compound 6 $[Fe_{0,684}Mn_{0,316}(PM\text{-}PEA)_2(NCS)_2]$ C 68.51, H 3.83, N 11.41, S 8.71. Found C 66.85, H 3.78, N 11.03, S 8.76. Calc. for Compound 7 $[Fe_{0,563}Mn_{0,437}(PM\text{-}PEA)_2(NCS)_2]$ C 68.52, H 3.83, N 11.41, S 8.71. Found C 66.56, H 3.75, N 11.00, S 8.70. Calc. for Compound 8 $[Fe_{0,476}Mn_{0,524}(PM\text{-}PEA)_2(NCS)_2]$ C 68.54, H 3.84, N 11.42, S 8.71. Found C 66.82, H 3.52, N 10.92, S 7.89. Calc. for Compound 9 $[Fe_{0,363}Mn_{0,637}(PM\text{-}PEA)_2(NCS)_2]$ C 68.54, H 3.84, N 11.42, S 8.71. Found C 66.91, H 3.55, N 10.91, S 7.45. Calc. for Compound 10 $[Mn(PM\text{-}PEA)_2(NCS)_2]$ C 68.56, H 3.84, N 11.42, S 8.72. Found C 67.22, H 3.78, N 11.23, S 8.98. A slight discrepancy is observed between the expected and found carbon ratio, probably due to the possible oxidation of the carbon-carbon triple bond of the ligand.

4. Physical Measurements

Chemical CHNS elemental analyses were performed on a FlashEA-1112 microanalyzer (ThermoFisher Scientific, Waltham, MA, USA) with a Mettler Toledo MX5 microbalance (Mettler Toledo, Viroflay, France). Powder X-ray diffraction data were recorded using a PANalytical X′Pert MPD diffractometer (Panalytical, Almelo, The Netherlands) with Bragg–Brentano geometry, Cu Kα radiation and a backscattering graphite 370 monochromator. Magnetic susceptibilities were measured in the 5–300 K temperature range, under an applied magnetic field of 1 T, using a MPMS5 SQUID magnetometer (Quantum Device, San Diego, CA, USA). The samples were precisely weighted and

corrections were applied to account for the compound and sample holder diamagnetic contributions. Photomagnetic measurements were performed using an 830 nm photodiode coupled *via* an optical fiber to the cavity of the SQUID magnetometer. The optical power at the sample surface was adjusted to 5 mW· cm^{-2}, and it was verified that this corresponds to a negligible change in the magnetic response due to the heating of the sample. Photomagnetic samples consisted of a thin layer of compound whose weight was obtained by comparison of the thermal SCO curve to that of a more accurately weighed sample of the same material. Our previously published standardized method for obtaining LIESST data [34–36] was followed. After slow cooling down to 10 K, the sample was irradiated and the change in magnetism was monitored. Once the saturation point was reached, the laser was switched off, and temperature was raised at 0.4 K· min^{-1}. During the heating ramp, magnetization was measured every 1 K. *T(*LIESST*)* was determined from the minimum of the $\partial\chi_M T/\partial T$ *vs.* T plot, as previously published [34–36]. In other experiments the sample was rapidly quenched at 10 K by inserting the sample holder (in less than 10 s) from room temperature down to the SQUID cavity previously cooled at 10 K. The same procedure as for *T(*LIESST*)* was then followed to record the *T*(TIESST).

5. External Pressure Investigated by Single-Crystal X-ray Diffraction

In situ pressure. The crystal structure at 55 MPa was determined from XRD data collected with a Bruker SMART CCD (Bruker AXS, Karlsruhe, Germany), the sample being placed in the laboratory-designed quartz pressure cell previously described [57]. In this case, the crystal is set up in a water-filled capillary. Higher pressure data were obtained using a diamond anvil cell (DAC) using a laboratory-designed Ahsbahs-type cell and a protocol described elsewhere [15,58]. The advantage of such DAC is the wide aperture angle (342°) allowing to almost collecting the full reciprocal space, which appears essential when dealing with low-symmetry crystal systems. The pressure dependence of the unit-cell was run on a Bruker-Nonius κ-CCD diffractometer, Mo-Kα radiation (0.71073 Å) at room temperature. The crystal was seriously damaged after 400 MPa, allowing the unit-cell determination but not a full crystal-structure determination. When the pressure was released, the sample was even more damaged preventing from any further analysis.

Ex situ pressure. Single crystals were put in a leak-free tank under controlled nitrogen gas pressure in the range [20–200 MPa] during 15 min each. The pressure was then release and crystals were directly mounted on a Bruker-Nonius κ-CCD diffractometer, Mo-Kα radiation (0.71073 Å) at 293 K, full data collection were run and the crystal structures refined starting from the referenced atomic parameters. The temperature dependence was done using an Oxford CryoSystem 700 (OxfordCryosystem, Oxford, United-Kingdom, 2001) installed on the diffractometer in the range 310–130 K at a cooling/warming rate of 2 K· min^{-1}. Crystals were very often damaged at the SCO for this compound (even with faster or slower cooling rates). For the investigation at 0.001 MPa the single-crystals were submitted to a primary vacuous for a few minutes. The experiment at 20 MPa was reproduced a few times, leading to the same results, and permitting to check the irreversibility of the modifications due to the pressure treatment after a few weeks.

6. Conclusions

Firstly, the present result shows that playing with pressure allows to modulate the SCO features of the [Fe(PM-PEA)$_2$(NCS)$_2$] compound; including the hysteresis width. Secondly, it opens the route to new characteristics such as the irreversible modifications of SCO temperatures or to a more effective photo-conversion rate. Thirdly, it reveals new aspects on this molecular compound that are interpreted as coming from metastable phases reached by a combination of internal pressure and temperature changes; the latter referring to quenching effects. Finally, it opens new questions such as for example the discrepancy of the SCO features modifications between the application of internal and external pressure; internal pressure decreasing the hysteresis width while the external pressure increases it.

This study probably marks the title compound as a peculiar one in the field of molecular iron SCO complexes but it also reinforces the need to examine SCO material under pressure. If the latter is

not only restricted to *in situ* and to high values but on the contrary taken in all its aspects, it therefore may be used to enhance SCO features and to get new structural phases; which can be envisaged as an alternative to the search for new SCO compounds.

Acknowledgments: The authors would like to thank the French network on Molecular Magnetism and Switching (GDR MCM2) for giving nice opportunities to present and discuss the results, the Groupement d'intérêt scientifique GIS-Advanced Materials in Aquitaine (AMA), the Aquitaine Region for supporting the development of the ICPA (International Center of Photomagnetism in Aquitaine) platform at Institut de Chimie de la Matière Condensée de Bordeaux (ICMCB), the X-Ray diffraction and the chemical analyses services of ICMCB and the center of characterization of materials (CECAMA).

Author Contributions: All authors contributed equally to the work. Guillaume Chastanet and Philippe Guionneau wrote the paper.

Conflicts of Interest: The authors declare no conflict of interest.

References

1. Tidey, J.; Wong, L.S.; Schröder, M.; Blake, A. Structural chemistry of metal coordination complexes at high pressure. *Coord. Chem. Rev.* **2014**, *227–278*, 187–207. [CrossRef]
2. Perutz, M.F.; Kilmartin, J.V.; Nagai, K.; Szabo, A.; Simon, S.R. Influence of globin structures on the state of the heme: Ferrous low spin derivatives. *Biochemistry* **1976**, *15*, 378–387. [CrossRef] [PubMed]
3. Weber, G.; Drickamer, H.G. The effect of high pressure upon proteins and other biomolecules. *Q. Rev. Biophys.* **1983**, *16*, 89–112. [CrossRef] [PubMed]
4. Di Primo, C.; Deprez, E.; Hoa, G.H.B.; Douzou, P. Antagonistic effects of hydrostatic pressure and osmotic pressure on cytochrome P-450cam spin transition. *Biophys. J.* **1995**, *68*, 2056–2061. [CrossRef]
5. McGammon, C.; Kantor, I.; Narygina, O.; Rouquette, J.; Ponkratz, U.; Sergueev, I.; Mezouar, M.; Prakapenka, V.; Dubrovinsky, L. Stable intermediate-spin ferrous iron in lower-mantle perovskite. *Nat. Geosci.* **2008**, *1*, 684–687. [CrossRef]
6. Ohnishi, S. A theory of the pressure-induced high-spin—Low-spin transition of transition-metal oxides. *Phys. Earth Planet. Int.* **1978**, *17*, 130–139. [CrossRef]
7. Ksenofontov, V.; Gaspar, A.B.; Gütlich, P. Pressure effect studies on spin crossover and valence tautomeric systems. In *Spin Crossover in Transition Metal Compounds III*; Gütlich, P., Goodwin, H.A., Eds.; Springer Berlin Heidelberg: Berlin, Germany, 2004; Volume 235, pp. 23–64.
8. Gütlich, P.; Gaspar, A.B.; Ksenofontov, V.; Garcia, Y. Pressure effect studies in molecular magnetism. *J. Phys. Condens. Matter* **2004**, *16*, S1087–S1108. [CrossRef]
9. Bonhommeau, S.; Molnár, G.; Goiran, M.; Boukheddaden, K.; Bousseksou, A. Theoretical study of the effect of an intense and pulsed magnetic field and a pressure pulse on the spin crossover complex $Fe(phen)_2(NCS)_2$. *Phys. Rev. B* **2006**, *74*, 064424/1–064424/8. [CrossRef]
10. Roux, C.; Zarembowitch, J.; Itié, J.P.; Polian, A.; Verdaguer, M. Pressure-induced spin-state crossovers in six-coordinate $Fe^{II}L_nL'_m(NCS)_2$ complexes with L = L′ and L ≠ L′: A XANES investigation. *Inorg. Chem.* **1996**, *35*, 574–580. [CrossRef]
11. Létard, J.-F.; Guionneau, P.; Goux-Capes, L. Towards spin crossover applications. In *Spin Crossover in Transition Metal Compounds III*; Gütlich, P., Goodwin, H.A., Eds.; Springer Berlin Heidelberg: Berlin, Germany, 2004; Volume 235, pp. 221–249.
12. Slichter, C.P.; Drickamer, H.G. Pressure-induced electronic changes in compounds of iron. *J. Chem. Phys.* **1972**, *56*, 2142–2160. [CrossRef]
13. Bousseksou, A.; Molnár, G.; Salmon, L.; Nicolazzi, W. Molecular spin crossover phenomenon: Recent achievements and prospects. *Chem. Soc. Rev.* **2011**, *40*, 3313–3335. [CrossRef] [PubMed]
14. Stoleriu, L.; Chakraborty, P.; Hauser, A.; Stancu, A.; Enachescu, C. Thermal hysteresis in spin-crossover compounds studied within the mechanoelastic model and its potential application to nanoparticles. *Phys. Rev. B* **2011**, *84*, 134102/1–134102/9. [CrossRef]
15. Guionneau, P.; Collet, E. Piezo- and Photo-Crystallography Applied to Spin-Crossover Materials. In *Spin-Crossover Materials: Properties and Applications*; Halcrow, M.A., Ed.; John Wiley & Sons Ltd.: Oxford, UK, 2013; pp. 508–526.

16. König, E.; Ritter, G.; Waigel, J.; Goodwin, H.A. The effect of pressure on the thermal hysteresis of the first-order spin transition in bis(1,10-phenanthroline-2-carbaldehyde phenylhydrazone) iron(II) complexes. *J. Chem. Phys.* **1985**, *83*, 3055–3061. [CrossRef]
17. Szilágyi, P.A.; Dorbes, S.; Molnár, G.; Real, J.A.; Homonnay, Z.; Faulmann, C.; Bousseksou, A. Temperature and pressure effects on the spin state of ferric ions in the [Fe(sal_2-trien)][Ni(dmit)$_2$] spin crossover complex. *J. Phys. Chem. Solids* **2008**, *69*, 2681–2686. [CrossRef]
18. Ksenofontov, V.; Levchenko, G.; Spiering, H.; Gütlich, P.; Létard, J.-F.; Bouhedja, Y.; Kahn, O. Spin crossover behavior under pressure of Fe(PM-L)$_2$(NCS)$_2$ compounds with substituted 2′-pyridylmethylene 4-anilino ligands. *Chem. Phys. Lett.* **1998**, *294*, 545–553. [CrossRef]
19. Bargeron, C.B.; Drickamer, H.G. Effect of pressure on the electronic structure of complexes of ferrous iron with substituted phenanthrolines. *J. Chem. Phys.* **1971**, *7*, 3471–3482. [CrossRef]
20. Long, G.J.; Hutchinson, B.B. Spin equilibrium in iron(II) poly(1-pyrazolyl)borate complexes: Low-temperature and high-pressure Mössbauer spectral studies. *Inorg. Chem.* **1987**, *26*, 608–613. [CrossRef]
21. Garcia, Y.; Ksenofontov, V.; Levchenko, G.; Schmitt, G.; Gütlich, P. Pressure-induced high spin state in [Fe(btr)$_2$(NCS)$_2$]· H$_2$O (btr = 4,4′-bis-1,2,4-triazole). *J. Phys. Chem. B* **2000**, *104*, 5045–5048. [CrossRef]
22. Ganguli, P.; Gütlich, P.; Müller, E.W. Effect of metal dilution on the spin-crossover behavior in [Fe$_x$M$_{1-x}$(phen)$_2$(NCS)$_2$] (M = Mn, Co, Ni, Zn). *Inorg. Chem.* **1982**, *21*, 3429–3433. [CrossRef]
23. Haddad, M.S.; Federer, W.D.; Lynch, M.W.; Hendrickson, D.N. An explanation of unusual properties of spin-crossover ferric complexes. *J. Am. Chem. Soc.* **1980**, *102*, 1468–1470. [CrossRef]
24. Haddad, M.S.; Federer, W.D.; Lynch, M.W.; Hendrickson, D.N. Spin-crossover ferric complexes: Unusual effects of grinding and doping solids. *Inorg. Chem.* **1981**, *20*, 131–113. [CrossRef]
25. Varma, V.; Fernàndes, J.R. An infrared spectroscopy study of the low-spin-high-spin transition in [Fe$_x$M$_{1-x}$(phen)$_2$(NCS)$_2$]. A composition-induced change in the order of the spin-state transition. *Chem. Phys. Lett.* **1990**, *167*, 367–370. [CrossRef]
26. Martin, J.-P.; Zarembowitch, J.; Dworkin, A.; Haasnoot, J.G.; Varret, F. Solid-state effects in spin transitions: Influence of iron(II) dilution on the magnetic and calorimetric properties of the series [Fe$_x$Ni$_{1-x}$(4,4′-bis(1,2,4-triazole))$_2$(NCS)$_2$].cntdot.H$_2$O. *Inorg. Chem.* **1994**, *33*, 2617–2623. [CrossRef]
27. Martin, J.-P.; Zarembowitch, J.; Bousseksou, A.; Dworkin, A.; Haasnoot, J.G.; Varret, F. Solid state effects on spin transitions: Magnetic, calorimetric, and Mossbauer-effect properties of [Fe$_x$Co$_{1-x}$(4,4′-bis(1,2,4-triazole))$_2$(NCS)$_2$].cntdot.H$_2$O mixed-crystal compounds. *Inorg. Chem.* **1994**, *33*, 6325–6333. [CrossRef]
28. Baldé, C.; Desplanches, C.; Gütlich, P.; Freysz, E.; Létard, J.-F. Effect of the metal dilution on the thermal and light-induced spin transition in [Fe$_x$Mn$_{1-x}$(bpp)$_2$](NCSe)$_2$: When T(LIESST) reaches $T_{1/2}$. *Inorg. Chim. Acta* **2008**, *361*, 3529–3533. [CrossRef]
29. Baldé, C.; Desplanches, C.; Nguyen, O.; Létard, J.-F. Complete temperature study of the relaxation from HS to LS state in mixed [Fe$_x$Zn$_{1-x}$(phen)$_2$(NCS)$_2$] systems (with x = 1, 0.73, 0.5, 0.32, 0.19, 0.04). *J. Phys. Conf. Ser.* **2009**, *148*, 012026/1–012026/9. [CrossRef]
30. Hauser, A. Light-induced spin-crossover and the high spin → low spin relaxation. *Top. Curr. Chem.* **2004**, *234*, 155–198.
31. Hauser, A.; Enachescu, C.; Daku, M.L.; Vargas, A.; Amstutz, N. Low-temperature lifetimes of metastable high-spin states in spin-crossover and in low-spin iron(II) compounds: The rule and exceptions to the rule. *Coord. Chem. Rev.* **2006**, *250*, 1642–1652. [CrossRef]
32. Hauser, A. Intersystem crossing in Fe(II) coordination compounds. *Coord. Chem. Rev.* **1991**, *111*, 275–290. [CrossRef]
33. Descurtins, S.; Gütlich, P.; Köhler, C.P.; Spiering, H.; Hauser, A. Light-induced excited spin state trapping in a transition-metal complex: The hexa-1-propyltetrazole-iron(II) tetrafluoroborate spin-crossover system. *Chem. Phys. Lett.* **1984**, *105*, 1–4. [CrossRef]
34. Létard, J.-F.; Guionneau, P.; Rabardel, L.; Howard, J.A.K.; Goeta, A.E.; Chasseau, D.; Kahn, O. Structural, magnetic and photomagnetic studies of a mononuclear iron(II) derivative exhibiting an exceptionally abrupt spin transition. Light induced thermal hysteresis phenomenon. *Inorg. Chem.* **1998**, *37*, 4432–4441. [CrossRef] [PubMed]
35. Létard, J.-F.; Capes, L.; Chastanet, G.; Moliner, N.; Létard, S.; Real, J.A.; Kahn, O. Critical temperature of the LIESST effect in iron(II) spin-crossover compounds. *Chem. Phys. Lett.* **1999**, *313*, 115–120. [CrossRef]

36. Létard, J.-F.; Chastanet, G.; Guionneau, P.; Desplanches, C. Optimising the stability of trapped metastable spin states. In *Spin-Crossover Materials—Properties and Applications*; Halcrow, M.A., Ed.; John Wiley & Sons: Chichester, UK, 2012; pp. 475–506.
37. Baldé, C.; Desplanches, C.; Wattiaux, A.; Guionneau, P.; Gütlich, P.; Létard, J.-F. Effect of metal dilution on the light-induced spin transition in $[Fe_xZn_{1-x}(phen)_2(NCS)_2]$ (phen = 1,10-phenanthhroline). *Dalton Trans.* **2008**, 2702–2707. [CrossRef]
38. Baldé, C.; Desplanches, C.; Grunert, M.; Wei, Y.; Gütlich, P.; Létard, J.-F. Influence of metal dilution on the light-induced spin transition in two 1D chain compounds: $[Fe_xZn_{1-x}(btzp)_3](BF_4)_2$ and $[Fe_xZn_{1-x}(endi)_3](BF_4)_2$ {btzp = 1,2-bis(tetrazol-1-yl)propane and endi = 1,2-Bis(tetrazol-1-yl)ethane}. *Eur. J. Inorg. Chem.* **2008**, 5382–5389. [CrossRef]
39. Paradis, N.; Chastanet, G.; Létard, J.-F. When stable and metastable HS states meet in spin-crossover compounds. *Eur. J. Inorg. Chem.* **2012**, 3618–3624. [CrossRef]
40. Paradis, N.; Chastanet, G.; Varret, F.; Létard, J.-F. Metal dilution of cooperative spin-crossover compounds: When stable and metastable high-spin states meet. *Eur. J. Inorg. Chem.* **2013**, 968–974. [CrossRef]
41. Paradis, N.; Chastanet, G.; Palamarciuc, T.; Rosa, P.; Varret, F.; Boukheddaden, K.; Létard, J.-F. Detailed investigation of the interplay between the thermal decay of the low temperature metastable HS state and the thermal hysteresis of spin-crossover solids. *J. Phys. Chem. C* **2015**, *119*, 20039–20050. [CrossRef]
42. Létard, J.-F.; Guionneau, P.; Codjovi, E.; Lavastre, O.; Bravic, G.; Chasseau, D.; Kahn, O. Wide thermal hysteresis for mononuclear spin-crossover compound *cis*-bis(thiocyanato)bis[*N*-(2′-pyridylmethylene)-4-(phenylethynyl)aniline] iron(II). *J. Am. Chem. Soc.* **1997**, *119*, 10861–10862. [CrossRef]
43. Guionneau, P.; Le Gac, F.; Lakhoufi, S.; Kaiba, A.; Chasseau, D.; Létard, J.-F.; Négrier, P.; Mondieg, D.; Howard, J.A.K.; Léger, J.-M. X-ray diffraction investigation of a spin-crossover hysteresis loop. *J. Phys. Condens. Matter* **2007**, *19*, 326211/1–326211/11. [CrossRef]
44. Guionneau, P. Crystallography and spin-crossover. A view of breathing materials. *Dalton Trans.* **2014**, *43*, 382–393. [CrossRef] [PubMed]
45. Le Gac, F.; Guionneau, P.; Létard, J.-F.; Rosa, P. The Zn polymorphic analogues of the $[Fe(PM–PEA)_2(NCS)_2]$ spin-transition compound. *Inorg. Chim. Acta* **2008**, *361*, 3519–3524. [CrossRef]
46. Legrand, V.; Pechev, S.; Létard, J.-F.; Guionneau, P. Synergy between polymorphism, pressure, spin-crossover and temperature in $[Fe(PM\text{-}BiA)_2(NCS)_2]$: A neutron powder diffraction investigation. *Phys. Chem. Chem. Phys.* **2013**, *15*, 13872–13880. [CrossRef] [PubMed]
47. Marbeuf, A.; Matar, S.F.; Négrier, P.; Kabalan, L.; Létard, J.-F.; Guionneau, P. Molecular dynamics of spin crossover: The (P, T) phase diagram of $[Fe(PM\text{-}BIA)_2(NCS)2]$. *Chem. Phys.* **2013**, *420*, 25–34. [CrossRef]
48. Jeftic, J.; Menéndez, N.; Wack, A.; Codjovi, E.; Linarès, J.; Goujon, A.; Hamel, G.; Klotz, S.; Syfosse, G.; Varret, F. Helium gas pressure apparatus with optical reflectivity detection. *Meas. Sci. Technol.* **1999**, *10*, 1059–1064. [CrossRef]
49. Marchivie, M.; Guionneau, P.; Létard, J.-F.; Chasseau, D. Towards direct correlations between spin-crossover and structural features in iron(II) complexes. *Acta Cryst. B* **2003**, *59*, 479–486. [CrossRef]
50. Létard, J.-F.; Kollmansberger, M.; Carbonera, C.; Marchivie, M.; Guionneau, P. Structural, magnetic and photomagnetic study of the $[Fe(PM\text{-}NEA)_2(NCS)_2]$ spin crossover complex. *C. R. Chim.* **2008**, *11*, 1155–1165. [CrossRef]
51. Halcrow, M.A. Structure: Function relationships in molecular spin-crossover complexes. *Chem. Soc. Rev.* **2011**, *40*, 4119–4142. [CrossRef] [PubMed]
52. Shatruk, M.; Phan, H.; Chrisostomo, B.A.; Suleimenova, A. Symmetry-breaking structural phase transitions in spin crossover complexes. *Coord. Chem. Rev.* **2015**, *289–290*, 62–73. [CrossRef]
53. Le Bail, A. Whole powder pattern decomposition methods and applications: A retrospection. *Powder Diffr.* **2005**, *20*, 316–326. [CrossRef]
54. Shannon, R.D. Revised effective ionic radii and systematic studies of interatomic distances in halides and chalcogenides. *Acta Cryst. A* **1976**, *35*, 751–767. [CrossRef]
55. Marchivie, M.; Guionneau, P.; Letard, J.-F.; Chasseau, D.; Howard, J.A.K. Thermal trapped iron(II) high spin state investigated by X-ray diffraction. *J. Phys. Chem. Solids* **2004**, *65*, 17–23. [CrossRef]
56. Pelleteret, D.; Clérac, R.; Mathonière, C.; Harté, E.; Schmitt, W.; Kruger, P.E. Asymmetric spin crossover behaviour and evidence of light-induced excited spin state trapping in a dinuclear iron(II) helicate. *Chem. Commun.* **2009**, 221–223. [CrossRef] [PubMed]

57. Yufit, D.S.; Howard, J.A.K. Simple pressure cell for single-crystal X-ray crystallography. *J. Appl. Cryst.* **2005**, *38*, 583–586. [CrossRef]
58. Guionneau, P.; Lepevelen, D.; Marchivie, M.; Pechev, S.; Gaultier, J.; Barrans, Y.; Chasseau, D. Laboratory high-pressure single-crystal X-ray diffraction—Recent improvements and examples of studies. *J. Phys. Condens. Matter* **2004**, *16*, 1129–1159. [CrossRef]